Dual receptor engagement by mannose-capped lipoarabinomannan reprograms macrophage lipid metabolism in tuberculosis

Dhubajyoti Nag[1], Joycelyn Radeny[1,2], Jinyan Cui[4], Omair Vehra [1,2], Yan Yu[4], Jérôme Nigou[5], Samantha L. Bell[1,2,3], Maria L Gennaro[1,6]*.

[1] Public Health Research Institute, Rutgers New Jersey Medical School, Newark, NJ, USA

[2] Center for Emerging and Re-emerging Pathogens, Rutgers New Jersey Medical School, Newark, NJ, USA

[3] Department of Microbiology, Biochemistry & Molecular Genetics, Rutgers New Jersey Medical School, Newark, NJ, USA

[4] Department of Chemistry, Department of Biomedical Engineering, Washington University in St. Louis, St. Louis, MO, USA

[5] Université de Toulouse, CNRS, Institut de Pharmacologie et de Biologie Structurale, Toulouse, France.

[6] Department of Medicine, Rutgers New Jersey Medical School, Newark, NJ, USA

***** To whom correspondence may be addressed. Email: gennarma@njms.rutgers.edu

Keywords: macrophages, lipid droplet, pathogen-associated molecular patterns, pattern recognition receptors.

Significance statement

Characterizing how lipid-laden foam cells arise is central to understanding tuberculosis pathogenesis, as these cells define the necrotizing lesions that drive lung damage and transmission. We show that mannose-capped lipoarabinomannan, a single mycobacterial component, engages two distinct immune receptors on macrophages to drive lipid metabolic reprogramming, demonstrating that one microbial entity can activate multiple receptor pathways through integrated signaling. This finding defines a broader principle whereby the structural architecture of a microbial ligand encodes multi-receptor engagement to shape host responses. By delineating receptor signal integration in foam cell formation, this work provides a mechanistic framework for tuberculosis pathogenesis and highlights host pathways that may represent targets for host-directed intervention.

Abstract

Necrotizing granulomas, the pathological hallmark of active tuberculosis, are characterized by the accumulation of lipid droplet-laden macrophage foam cells that promote tissue destruction, bacterial persistence, and transmission. Despite their central role in tuberculosis pathogenesis, the molecular mechanisms driving foam cell formation remain poorly defined. Here, we demonstrate that the mannose-capped lipoglycan lipoarabinomannan (ManLAM), a major mycobacterial virulence factor, induces macrophage lipid droplet accumulation through coordinated engagement of Toll-like receptor 2 and Dectin-2. Distinct structural moieties within ManLAM are selectively required for recognition by each receptor. Dual receptor engagement synergistically enhances both lipid metabolic reprogramming and NF-κB-mediated inflammatory signaling. However, lipid accumulation proceeds through an mTORC1-PPARγ-dependent pathway that is largely independent of inflammatory activation. ManLAM-induced lipid metabolic changes closely mirror those elicited during *Mycobacterium tuberculosis* infection, both in triglyceride composition and in dependence on the mTORC1-PPARγ axis. These findings identify ManLAM as a major mycobacterial input into foam cell-associated lipid metabolism and delineate how a single microbial ligand, through coordinated engagement of two distinct innate immune receptors, couples mycobacterial recognition to macrophage lipid metabolism reprogramming.

Introduction

Tuberculosis (TB) remains the leading cause of death from a single infectious agent worldwide (1). Infection with *Mycobacterium tuberculosis* drives the formation of lung granulomas -- organized multicellular structures that initially restrict bacterial dissemination but, under sustained immune stimulation, can progress to necrotizing lesions (2-4). These necrotizing granulomas, the pathological hallmark of active TB, underlie lung tissue destruction, impaired respiratory function, and transmission of infection upon release of infectious material into the airways (2-4). A defining cellular event in this pathological transition is the emergence of foam cells, macrophages characterized by the accumulation of cytosolic lipid droplets enriched in triglycerides (4). In TB, foam cells promote disease progression by exhibiting impaired antimicrobial activity, amplifying pro-inflammatory and pro-necrotic signaling, and contributing directly to the necrotic core upon cell death (4, 5). In addition, they may serve as a lipid reservoir that supports *M. tuberculosis* persistence and sequesters lipophilic antibiotics such as bedaquiline (5, 6). In TB, foam cell formation represents a point of convergence between immune activation, metabolic remodeling, and tissue pathology. Despite their central role at the interface of inflammation, metabolism, and pathology, the molecular mechanisms that drive foam cell biogenesis in TB remain poorly defined.

Multiple mycobacterial components -- predominantly associated with the cell envelope -- have been linked to macrophage lipid droplet accumulation. Mannose-capped lipoarabinomannan (ManLAM) is the best-characterized of these factors. ManLAM is a ~17-kDa structurally highly heterogeneous lipoglycan composed of a mannosyl-phosphatidylinositol anchor, a mannan core, and an arabinan domain capped with terminal mannose residues in pathogenic mycobacteria, including the *M. tuberculosis* complex (7-9). In addition to its structural role in cell wall integrity (10), ManLAM is a major determinant of mycobacterial virulence, disrupting macrophage phagosome maturation and modulating adaptive immune responses**,** including CD1-restricted T cell activation, $CD4^+$ T cell function, and cytokine and antibody production by B cells (8, 9, 11, 12). Such pleiotropic effects are consistent with ManLAM's capacity to engage multiple pattern-recognition receptors on macrophages, including C-type lectin receptors such as the mannose receptor and Dectin-2 -- with high avidity for the latter (13, 14) -- as well as Toll-like receptor 2 (TLR2), albeit with low affinity (15, 16). Seminal work by D'Avila *et al* (17) demonstrated that TLR2 is required for ManLAM-induced lipid droplet accumulation. However, a potent TLR2 agonist fails to induce this response (18). Together,

these observations reveal that TLR2 signaling is necessary but insufficient to promote foam cell formation, leaving unresolved how ManLAM drives lipid droplet biogenesis.

In the present work, we identify coordinated engagement of TLR2 and Dectin-2 as the mechanistic principle underlying ManLAM-driven foam cell formation. ManLAM integrates signals from these two pattern-recognition receptors to activate an mTORC1-PPARγ axis that drives triglyceride synthesis and lipid droplet biogenesis in macrophages. This signal integration is achieved via distinct structural moieties of the ManLAM molecule, which are also required for synergistic induction of inflammatory responses. By defining the structural determinants of ManLAM activity, the receptor-level requirements, and the downstream metabolic signaling pathways involved, our findings reveal how a single mycobacterial factor couples inflammatory recognition to metabolic reprogramming. Together, these results establish a mechanistic framework for foam cell formation in TB and identify host pathways that may represent points of vulnerability for host-directed therapeutic intervention.

Materials and Methods

Mycobacterial strains and purified components

Mycobacterium tuberculosis Erdman (TMC#107) was cultured in complete 7H9 medium, which consists of Middlebrook 7H9 base (BD Difco, Franklin Lakes, NJ) supplemented with 10% (v/v) oleic acid-albumin-dextrose-catalase (OADC) obtained from oleic acid (0.5 g/L, Thermo Fisher Scientific, Waltham, MA), albumin (50 g/L), dextrose (20 g/L), and catalase (0.04 g/L all from Fisher Scientific, Hampton, NH). The medium also contained sodium chloride (8 g/L), glycerol (0.5% v/v), and was supplemented with 0.05% tyloxapol (all from Thermo Fisher Scientific, Hampton, NH).

Mannosylated lipoarabinomannan (ManLAM) was extracted from *M. tuberculosis* Erdman and purified by a previously described method (51). Deacylated ManLAM (dManLAM) was prepared as described previously (52). Briefly, 200 µg of ManLAM was incubated in 200 µl of NaOH 0.1 M for 2 h at 37°C. After neutralization with 200 µl of HCl 0.1 M, the reaction products were dialyzed against water. ManLAM devoid of mannose caps (αtManLAM) was prepared as described previously (53). Briefly, 200 µg of ManLAM was incubated for 6 h at 37°C in 30 µl of α-mannosidase solution (2 mg/ml, 0.1 M sodium acetate buffer, pH 4.5, 1 mM $ZnSO_4$) followed by a second addition of 50 µl of the same enzyme solution for overnight incubation at 37°C. The

reaction products were dialyzed against 50 mM NH_4CO_3, pH 7.6. Elimination of α-mannosidase was achieved by denaturation (2 min at 110°C) followed by overnight tryptic digestion with trypsin/α-mannosidase (2% by weight) at 37°C. αtManLAM was recovered after dialysis against water. Removal of mannose caps was controlled by capillary electrophoresis as described earlier (52). dManLAM and αtManLAM were suspended in 1x phosphate buffer saline (PBS) pH 7.4 and stored at -20°C. To inactivate putative lipoprotein contaminating ManLAM and its derivatives, samples were incubated with 1% H_2O_2 for 3h at 37°C, a treatment that converts the N-terminal cysteine-thioether substructure of lipoproteins into TLR-2-inactive sulfoxide derivatives (19). At the end of the incubation period, H_2O_2 was evaporated under N_2 gas and the resulting pellets were reconstituted in distilled H_2O.

Cell lines

Murine bone marrow marrow-derived macrophages obtained from C57BL/6 mice and immortalized with J2 retrovirus (iBMDMs) (54) were kindly provided by Dr. Phillip West (Jackson Laboratory, Bar Harbor, ME). iBMDMs were cultured in Dulbecco's modified Eagle's medium (DMEM) supplemented with heat-inactivated 10% FBS, 1x penicillin-streptomycin solution (100 IU/mL penicillin and 100 µg/ml Streptomycin; Corning, Manassas, VA) and 20 mM HEPES (Millipore, Billerica, MA) and incubated at 37°C in a humidified atmosphere consisting of 5% CO_2. RAW264.7 cells carrying an EGFP-RelA reporter (55) were cultured in DMEM containing 10% FBS, 2 mM l-glutamine, 1x penicillin-streptomycin solution (Corning, Manassas, VA), and 10 mM HEPES (Millipore, Billerica, MA) at 37°C and 5% CO_2. The HEK-Blue mDectin-2 and HEK-Blue hTLR2 (InvivoGen, San Diego, CA) are derivatives of HEK293 cells that stably express the murine Dectin-2 and the human TLR2 genes, respectively, along with a NF-κB-inducible reporter system (secreted alkaline phosphatase). These cells were maintained in DMEM containing 10% FBS, 4.5 g/l glucose, 2 mM L-glutamine, 1x penicillin-streptomycin solution, 100 µg/ml zeocin, 200 µg/ml hygromycin, 10 µg/ml blasticidin, 1 µg/ml puromycin, and 1x TLR and CLR Selection solution (all from InvivoGen, San Diego, CA). Reporter cells were cultured for two passages without selection before use.

Gene knock-down (KD) in iBMDMs

iBMDMs were transduced with lentivirus carrying nuclease-dead FLAG-tagged Cas9 (dCas9) and selected for using blasticin (5-10 μg/ml) (InvivoGen, San Diego, CA). The Lenti-dCas9-KRAB-blast plasmid was a gift from Gary Hon (U. Texas South Western) (Addgene plasmid # 89567; http://n2t.net/addgene:89567) (20). For each gene of interest, 5-6 small guide RNAs (sgRNAs) were selected using the CRISPick tool (Broad Institute, https://portals.broadinstitute.org/gppx/crispick/public) (21, 22). sgRNAs were cloned into the pLentiGuide-Puro backbone, which was a gift from Paul Khavari (Stanford U.) (Addgene plasmid # 117986; http://n2t.net/addgene:117986). dCas9-containing cells were transduced with lentivirus carrying gene-specific sgRNAs and selected for by using puromycin (5-10 μg/ml) (InvivoGen, San Diego, CA). Non-targeting sgRNAs (targeting *luxA*) were used as negative controls: *lux1*: GGCAATGAAACGCTACGCTC, *lux2*: ATAAAGAGCGCGCCCAACAC. Knockdown cells were validated by RT-qPCR, and the cell lines carrying the two gene-specific sgRNAs with the highest knockdown efficiency were used for subsequent experiments. The gene-specific sgRNAs used in this study were: TLR2-1: TGGGTGTCCCTCTTCCTGCA, TLR2-2: AAGCTGATCCGCCCGGCTGG; Dectin-2-1: GGACCTGGCTTCTGTCAAAG, Dectin-2-2: TGAGTTAAATGCCACAGAGC. For both steps of transduction, lentivirus was produced using HEK293T-Lenti-X cells (Takara) and psPAX2 (Addgene plasmid #12260; http://n2t.net/addgene:12260) and pMD2.G/VSV-G (Addgene plasmid #12259; http://n2t.net/addgene:12259) packaging plasmids, which were gifts from Didier Trono (EPFL, Swiss Federal Technology Institute of Lausanne).

***M. tuberculosis* infection**

M. tuberculosis strain mc^{2}6206 ($H_{37}Rv$ *ΔpanCD ΔleuCD*) was kindly provided by Dr. William Jacobs Jr. (Albert Einstein College of Medicine) (23). This strain was grown in Middlebrook 7H9 supplemented with 10% OADC, 0.5% glycerol, 0.05% Tween-80, 24 ug/ml pantothenate, 50 ug/ml leucine, and 0.1 mM propionate. Macrophage infections were performed as previously described (24, 25). Briefly, *M. tuberculosis* cultures were grown to an OD_{600} of 0.6-1.0, washed three times with PBS, and centrifuged at 500 x *g* for 5 min to remove clumps. Bacteria were diluted in DMEM plus 10% horse serum and added to iBMDMs plated at 3-4x10^5 cells/well in a 12-well dish in iBMDM media containing 24 ug/ml pantothenate and 50 ug/ml leucine. A diluted bacterial inoculum was added to cultured iBMDM (MOI = 15), and cells were centrifuged at

1,000 x *g* for 10 min to synchronize the infection and resuspended in fresh iBMDM media containing 24 ug/ml pantothenate and 50 ug/ml leucine; culture media was changed daily. After 48 h, iBMDMs were detached from tissue culture plates by resuspending in 1 x PBS plus 4mM EDTA by gentle scraping. An equal volume of 8% paraformaldehyde was added to fix and inactivate the samples. Cells were washed twice with 1 x PBS and processed for LD formation as described below.

Chemical reagents and antibodies

TLR2 ligand Pam3CSK4 and Dectin-2 ligand furfurman were purchased from Invivogen (San Diego, CA). Inhibitors of diacylglycerol transferase (A922500) and acyl-coenzyme A:cholesterol acyltransferase (CAS 615264-52-3), both from Santa Cruz Biotechnology, Dallas, TX, were stored as per manufacturer's instructions. Inhibitors of Mechanistic Target of Rapamycin Complex 1 (Rapamycin), peroxisome proliferator-activated receptor gamma (GW9662), NF-κB (JSH-23, QNZ, and BAY 11-7082) were all from Selleckchem, Houston, TX. Inhibitor doses were selected at and around published EC_{50} data and toxicity profiles in macrophages (26-28). Only inhibitor doses yielding >85% cell viability were utilized by using trypan blue (Cytiva, Marlborough, MA) and counting with an automated cell counter (LUNA-FX7, Logos Biosystem, Annandale, VA). Mouse Fc receptor blocking solution, anti-mouse CD16/CD32, BV421 rat anti-mouse F4/80 (BD Biosciences, San Diego, CA) and Bodipy 493/503 (Life Technologies, Carlsbad, CA) were used at the dilutions suggested by the manufacturers and as per previous work (26).

TLR2 and Dectin-2 reporter cell experiments

The HEK-Blue reporter cell experiments were performed following manufacturer's protocols (13), with minor modifications. For the HEK-Blue hTLR2 reporter assay, 20 µl of ManLAM, αtManLAM, dManLAM, and Pam3CSK4 (TLR2 ligand), all suspended in 1x PBS, were added to each well in 96-well plates (in triplicate) to obtain a final concentration of 5 µg/ml of each reagent. HEK-Blue hTLR2 cells were harvested, washed in 1x PBS, and resuspended in Quanti-Blue media (InvivoGen, San Diego, CA) at a final density of 280,000 cells/ml. 180 µl of cell suspension was added to each well and incubated for 24 h at 37°C in a humidified atmosphere containing 5% CO_2. For the HEK-Blue mDectin-2 reporter assay, 10 µl of ManLAM,

αtManLAM, dManLAM and furfurman (Dectin-2 ligand) were suspended in 1x PBS and added to each well in 96-well plates (in triplicate) to obtain a final concentration of 10 µg/ml for ManLAM and derivatives and 200 µg/ml for furfurman. The plates were dried at 37°C until the solvent evaporated (~3 h). HEK-Blue mDectin-2 cells were harvested, washed in 1x PBS, and resuspended in Quanti-Blue media at a final density of 280,000 cells/ml. 200 µl of cell suspension was added to each well and incubated for 24 h at 37°C in a humidified atmosphere containing 5% CO_2. For both reporter cell lines, the colorimetric reading was taken at 650 nm (OD_{650}). The data were expressed as OD_{650} ratio between treated cells and vehicle control cells.

Lipid droplet measurements

One million iBMDM cells in 1 ml culture medium were added to each well of 12-well tissue culture plates and incubated for 2 h at 37°C in a humidified atmosphere containing 5% CO_2. *M. tuberculosis* components and control agonists were diluted in the same medium and 1 ml of each suspension or solution was added to each well to obtain final concentrations of 500 ng/ml for ManLAM, ManLAM derivatives, and Pam3CSK4, and 10 µg/ml for furfurman. Treated and vehicle control cells were incubated for 24 h at 37°C in a humidified atmosphere containing 5% CO_2. When appropriate, chemical inhibitors were added at the indicated doses in a 10 µl solution, concurrently with the treatments above.

After incubation, cells were subjected to imaging flow cytometry as previously described (56). Briefly, medium was discarded and 1 ml 1x PBS was added to each well. iBMDM were detached from culture plates by gentle scraping, pelleted by centrifugation at 350g for 5 min, and fixed with 4% paraformaldehyde in 1x PBS for 45 min at RT. Cells were washed with 1x PBS containing 0.1% bovine serum albumin (PBS-BSA), resuspended in 50 µl of PBS-BSA containing 5 µl of mouse Fc-receptor blocking solution, and incubated at RT for 7 min. After incubation, 50 µl of PBS-BSA containing 5 µl of mouse F4/80-BV421 antibody were added to each tube, and samples were incubated for 30 min at 4°C. After washing with PBS-BSA, cells were stained with 0.3 µg/ml Bodipy 493/503 in 1x PBS for 15 min. For each condition, data were acquired from 5,000–10,000 F4/80-positive cells utilizing an ImageStreamXMark II imaging flow cytometer (Amnis Corporation, Seattle, WA), using 60x magnification. Image data were analyzed by IDEAS software version 6.0 (Amnis Corporation, Seattle, WA) after applying a compensation matrix and selecting the region of interest (lipid droplets) with the Spot Mask tool.

Mean fluorescence intensity (MFI) and spots per cell were extracted and expressed as ratio of treated vs its vehicle control cells.

Real Time PCR analysis

RNA was isolated using RNeasy Mini Kit (Qiagen, Valencia, CA, USA). Isolated RNA was subjected to cDNA synthesis using the SuperScriptTM First-Strand Synthesis System (Bio-Rad, Hercules, CA). Real time PCR was performed in a QuantStudio 7 Flex Real-Time time PCR machine (Thermo Fisher Scientific, Waltham, MA, USA) using the ABsolute QPCR SYBER Green Mix (ABgene, Rochester, NY, USA), according to the standard ABgene protocol. The sequence of the primers used for real time PCR are listed in **SI Table 1**. The internal control gene β-Actin was amplified simultaneously in a separate reaction. The threshold cycle number (CT) was determined by qPCR for triplicate reactions, and the mean CT of the triplicate reactions was calculated. Levels of expression of the genes of interest were normalized to β-Actin using the formula $2^{-\Delta DCT}$, where –ΔDCT = ΔCT (treated) – ΔCT (control), and ΔCT is the CT of the target gene subtracted from the CT of the housekeeping gene β-Actin.

Measurements of RelA nuclear translocation (NF-κB activation)

For the Rel-A nuclear translocation assay, RAW264.7 cells carrying a EGFP-RelA reporter gene fusion were plated at 4×10^5 cells per well in a 96-well glass-bottom plate overnight and then serum starved for 3 h. Cells were stimulated with the same treatments used for lipid accumulation experiments, and incubated for 0.5, 1.0, 1.5 and 2.0 h at 37°C. For fixed cell imaging, cells were fixed after stimulation with 2% PFA on ice for 5 min. Nuclei were counterstained with 2 μg/mL Hoechst stain at RT for 15 min. Fluorescence images were acquired using a Nikon Eclipse Ti microscope equipped with an Andor iXon3 EMCCD camera and a Nikon Plan Apo 40×/0.95 objective. For each sample, 20 images were taken at different locations. Images were analyzed using ImageJ following a previously reported method (55).

Statistical analysis

All values are presented as means ± standard deviation (SD) for technical triplicates. Comparisons between two groups were performed using a two-tailed Student's t-test in the

Prism graphpad software or by one-way ANOVA. The criterion for statistical significance was $p < 0.05$.

Results

M. tuberculosis ManLAM induces lipid droplet (LD) accumulation in mouse macrophages through TLR2 and Dectin-2 signaling.

ManLAM is a structurally heterogeneous lipoglycan comprising a defined class of biosynthetically related molecular species (7-9). Throughout this study, "ManLAM" refers to this molecular class rather than a single chemically uniform species. Previous studies showed that the vaccine strain *Mycobacterium bovis* Bacillus Calmette-Guérin (BCG), a member of the *M. tuberculosis* complex, induces LD accumulation in murine macrophages in a TLR2-dependent manner, yet activation of TLR2 alone by the synthetic agonist Pam3Cys (PAM3CSK4) is insufficient to induce LD formation (17, 18). Similar results were obtained with BCG-derived ManLAM (17, 18). These observations left unresolved how whole BCG cells – and specifically ManLAM – promote LD biogenesis in macrophages. Because ManLAM is a relatively weak TLR2 agonist compared to bacterial lipoproteins (EC_{50} is in the µg/ml *vs* ng/ml range) (15, 29), it was important to exclude the possibility that the observed TLR2-stimulating activity of the ManLAM preparation resulted from trace contamination with highly active lipopeptides (30). To address this, purified ManLAM was treated with 1% H_2O_2, which inactivates lipoproteins by converting the N-terminal cysteine-thioether substructure required for TLR2 activation into sulfoxide derivatives (19). Untreated and H_2O_2-treated ManLAM were tested with a TLR2 reporter HEK293 cell line engineered to express alkaline phosphatase activity as a read-out of TLR2-dependent NF-κB activation (see *Methods*). H_2O_2 treatment had little effect on the TLR2 agonist activity of *M. tuberculosis* ManLAM (**Fig. 1A**) while completely abrogating TLR2 activation by the sentinel lipoprotein LrpG (**SI Fig. 1B**). This result demonstrates that our ManLAM preparations are highly purified and express bona fide TLR2 agonism.

Next, to investigate the mechanisms underlying ManLAM-induced LD accumulation in macrophages, we used immortalized murine bone marrow-derived macrophages (iBMDMs), which are well suited for genetic manipulations and closely recapitulate primary macrophage phenotypes (31). Gene knockdown in iBMDMs was achieved by CRISPR-interference (CRISPRi), which employs a nuclease-inactivated Cas9 (dCas9) and promoter-targeting guide

RNAs (gRNAs) to block transcription of target genes. We generated TLR2 knockdown iBMDMs by stably expressing dCas9 together with two different gRNAs targeting the *Tlr2* promoter (see *Methods*). Control cells expressed gRNAs against an irrelevant target gene (bacterial luciferase, *lux*A). Efficient TLR2 knockdown was confirmed by reduced *Tlr2* transcript levels measured by RT-qPCR (**SI Fig 2A**) and by impaired induction of TLR2-responsive genes *Il6* and *Tnfa* following stimulation with the TLR2 agonist Pam3CSK4 (**SI Fig. 2B,C**). ManLAM and H_2O_2-treated ManLAM induced LD accumulation in control iBMDMs but failed to do so in TLR2 KD cells (**Fig. 1B**; representative imaging flow cytometry data in **Fig. 1C**). Moreover, in agreement with previous reports (18), stimulation of control iBMDMs with Pam3CSK4 alone failed to induce LD accumulation at any of the doses tested (**Fig. 1B-E**). The observed insufficiency of TLR2 signaling prompted us to investigate whether ManLAM engages other host receptors to drive macrophage LD accumulation.

Previous work has shown that *M. tuberculosis* ManLAM is also an agonist of Dectin-2 (13, 14), a surface C-type lectin receptor (CLR) that recognizes microbial carbohydrates and has been studied primarily in the context of fungal infections (32). Consistent with these reports, *M. tuberculosis* ManLAM activated Dectin-2 signaling in a reporter HEK293 cell line engineered to express alkaline phosphatase activity as a read-out of Dectin-2-dependent NF-κB activation (see *Methods*) (**Fig. 2A**). H_2O_2 treatment had no significant effect on the Dectin-2 agonist activity of *M. tuberculosis* ManLAM (**Fig. 2A**). To assess whether Dectin-2 signaling contributes to ManLAM-induced LD accumulation, we generated Dectin-2 knockdown (KD) and control cells in iBMDM using the same strategy described for TLR2. Efficient Dectin-2 knockdown was validated by reduced *Dectin2* transcript levels measured by RT-qPCR (**SI Fig. 2D**) and by impaired induction of the downstream genes *Il6* and *Tnfa* following stimulation with the Dectin-2 agonist furfurman (**SI Fig. 2E,F**). When LD induction was assessed, both ManLAM and H_2O_2-treated ManLAM induced LD accumulation in control iBMDM but failed to do so in Dectin-2 KD cells (**Fig. 2B**; representative imaging flow cytometry data are in **Fig. 2C**). In contrast, knockdown of other CLRs, including Dectin-1 and Mincle, had no effect on ManLAM-induced LD accumulation (**SI Fig. 3**). Moreover, treating iBMDMs with increasing doses of furfurman up to 10 μg/ml failed to induce LD accumulation (**Fig. 2D**). Thus, as observed with TLR2, Dectin-2 activation is necessary but insufficient to drive ManLAM-induced LD accumulation.

The data above strongly suggest that *M. tuberculosis* ManLAM engages both TLR2 and Dectin-2 signaling to induce LD accumulation in macrophages. To determine whether co-engagement of these two receptors is sufficient, we treated iBMDMs with the TLR2 agonist

Pam3CSK4 and the Dectin-2 agonist furfurman, alone and in combination. While neither agonist induced LD accumulation when applied alone, they did so when used in combination (**Fig. 3A**; representative imaging flow cytometry data are in **Fig. 3B**). These results demonstrate that co-engagement of TLR2 and Dectin-2 is sufficient to induce macrophage lipid droplet accumulation and raise the possibility that ManLAM functions as a single ligand coordinating signaling through both receptors to drive macrophage lipid reprogramming.

We next asked whether specific ManLAM structural features are required for lipid droplet accumulation mediated by TLR2 and Dectin-2. Prior work showed that acylation of the phosphatidyl-myo-inositol anchor of mycobacterial lipoglycans is required for TLR2 activation (16, 33), whereas the mannose caps of ManLAM are required for recognition by Dectin-2 (13, 14). To selectively disrupt these interactions, we generated deacylated ManLAM by NaOH treatment (dManLAM, see *Methods*) and mannose-cap-deficient ManLAM by enzymatic removal with α-mannosidase (αtManLAM, see *Methods*). When tested in TLR2 and Dectin-2 reporter HEK293 cell lines, dManLAM failed to activate TLR2 while retaining Dectin-2 activation ability (**Fig. 3C**). In contrast, αtManLAM retained TLR2 activation but lost the ability to activate Dectin-2 (**Fig. 3C**). We next assessed the ability of these ManLAM derivatives to induce LD accumulation in iBMDMs. In contrast to intact ManLAM, neither αtManLAM nor dManLAM induced LD accumulation (**Fig. 3D**; representative imaging flow cytometry data are in **Fig. 3E**). Together, these results demonstrate that simultaneous engagement of TLR2 and Dectin-2 by ManLAM is required for macrophage LD accumulation and identify the specific structural moieties of ManLAM that mediate this dual receptor recognition**.**

Intact *M. tuberculosis* ManLAM is required for maximal NF-κB activation

To quantitatively assess potential synergism between TLR2- and Dectin-2-dependent signaling elicited by ManLAM, we examined activation of the transcription factor NF-κB. Whereas the lipid droplet assay established requirement of both TLR2 and Dectin-2, it does not permit precise quantification of signaling synergy. NF-κB activation, which is known to be induced by ManLAM (13), provides a well-defined and quantitative readout downstream of multiple innate immune receptors, including Toll-like receptors (TLRs) and C-type lectin receptors (CLRs) (34). Upon receptor engagement, NF-κB is rapidly phosphorylated and translocates from the cytoplasm to the nucleus (schematic in **Fig. 4A**), where it induces expression of proinflammatory cytokines such as TNF-α (35). We therefore quantified NF-κB

activation by measuring nuclear translocation of the RelA (p65) subunit in macrophages treated with ManLAM or its structural derivatives.

Nuclear translocation was calculated as the ratio of nuclear to cytoplasmic RelA fluorescence intensity in RAW264.7 macrophages stably expressing green-fluorescence-protein -tagged RelA. Stimulation with ManLAM induced a gradual increase in nuclear RelA accumulation over time relative to unstimulated control cells (**Fig. 4B,C**). As expected, ManLAM-induced NF-κB activation was substantially less potent than that triggered by soluble Pam3CSK4, a benchmark agonist for robust TLR2-mediated activation.

Notably, ManLAM-induced RelA translocation exhibited substantial cell-to-cell variability, consistent with intrinsic heterogeneity in immune cell activation (36). To quantify this response, we defined a threshold that classified 95% of unstimulated cells as nonresponsive. Using this criterion, the macrophage population segregated into two groups: a responsive subpopulation displaying robust nuclear RelA accumulation and a nonresponsive subpopulation below the threshold (**SI Fig. 4**). Compared with intact ManLAM, αtManLAM and dManLAM reduced the fraction of responsive cells by approximately 50-60% (**Fig. 4D,E**) and diminished the magnitude of RelA translocation among responsive cells (**Fig. 4F**), indicating attenuated NF-κB activation at both the population and single-cell levels. Given the relationships established above between mannose capping, MPI acylation, and Dectin-2 and TLR2 recognition, we conclude that maximal NF-κB activation requires simultaneous engagement of both receptors by intact ManLAM. Consistent with this conclusion, 6-hr stimulation of iBMDMs with intact ManLAM induced eightfold greater TNF-α production than with either structural derivative (**SI Fig. 5**).

TLR2 and Dectin-2 are required for maximal LD accumulation during *M. tuberculosis* infection

To assess the relevance of our findings with purified ManLAM in the context of live *M. tuberculosis* infection, we examined the requirement for TLR2 and Dectin-2 signaling in macrophage LD accumulation during infection. Macrophages with knockdown of TLR2 or Dectin-2 exhibited an ~35% reduction in LD content following infection compared with parental cells (**Fig. 5A,B**). Thus, reduced expression of either receptor attenuated LD accumulation, indicating that both are required for maximal lipid storage during infection. Moreover, these results suggest that ManLAM constitutes a substantial, though not exclusive, contributor to the LD-inducing capacity of the pathogen.

ManLAM induces triglyceride-rich LDs via an mTORC1 and PPARγ axis independent of NF-κB

We next investigated whether ManLAM-induced macrophage LD accumulation resembles that observed during live *M. tuberculosis* infection. To define the chemical nature of the ManLAM-induced neutral lipids, untreated and ManLAM-treated iBMDMs were exposed to chemical inhibitors of diacylglycerol acyltransferase (DGAT), which converts di- into tri-glycerides, or acyl-CoA:cholesterol acyltransferase (ACAT), which esterifies free cholesterol. Inhibition of DGAT, but not ACAT, reduced ManLAM-induced LD accumulation in a dose-dependent manner (**Fig. 5C,D**), indicating that ManLAM induces triglyceride-enriched LDs, consistent with our prior findings with *M. tuberculosis* infection (26).

We next examined the signaling pathways underlying ManLAM-induced LD formation. Previous work showed that LD accumulation during tuberculous mycobacterial infection requires the protein kinase Mechanistic Target of Rapamycin Complex 1 (mTORC1) and the downstream transcription factor peroxisome proliferator-activated receptor gamma (PPARγ) (18, 26, 37). Both are key regulators of cellular lipid metabolism (38-40). Inhibition of mTORC1 with rapamycin or of PPARγ with GW9662 markedly reduced ManLAM-induced LD accumulation in a dose-dependent manner (**Fig. 5E**), recapitulating findings in *M. tuberculosis* infection (18, 26, 37). In contrast, although ManLAM activates NF-κB, LD accumulation was unaffected by inhibition of RelA (p65) nuclear translocation by JSH-23 (**Fig. 5E**). Similar results were obtained with two additional NF-κB inhibitors, BAY 11-7082 and QNZ (**SI Fig. 6**), indicating that Man-LAM-induced LD formation is independent of NF-κB activity.

To delineate pathway specificity, we examined how inhibition of mTORC1 and NF-κB altered expression of ManLAM-induced genes representing each signaling pathway. Rapamycin selectively inhibited ManLAM-mediated upregulation of the PPARγ target gene *Plin2*, which encodes a lipid droplet-associated protein (41), but did not affect induction of the NF-κB-regulated gene *Il1b* (42) (**Fig. 5F**). Conversely, the NF-κB inhibitor JSH-23 suppressed LAM-mediated induction of *Il1b* induction but not of *Plin2*. Both rapamycin and JSH-23 reduced ManLAM-induced upregulation of *Hif1a*, a gene controlled by both NF-κB and mTORC1 (43, 44)}. These results demonstrate that LD accumulation induced by ManLAM proceeds through an mTORC1-PPARγ-dependent metabolic program that is mechanistically independent of NF-κB signaling, mirroring the pathway architecture observed during *M. tuberculosis* infection (26, 45).

Discussion

Foam cells are the cellular hallmark of necrotizing TB lesions (26), yet how mycobacterial signals integrate to drive macrophage lipid metabolic reprogramming remains unresolved. Here we identify ManLAM as a major structural determinant of foam cell formation and show that its lipid-inducing activity requires coordinated engagement of TLR2 and Dectin-2. Distinct structural features of ManLAM -- acylation and mannose capping -- required for activation of each receptor (13, 14, 16, 33) are jointly necessary to drive triglyceride-rich lipid droplet accumulation. These findings define the mechanistic basis for the previously unexplained observation that TLR2 signaling is necessary but insufficient for lipid droplet formation. Although dual receptor engagement enhances NF-κB activation, lipid metabolic reprogramming proceeds through an mTORC1-PPARγ axis largely independent of inflammatory signaling. Together, these data support a model in which ManLAM co-engages two macrophage surface receptors through distinct moieties to induce lipid metabolic reprogramming and inflammatory activation via mechanistically separable pathways (**Fig. 6**). We further show that, as the sole *M. tuberculosis*–derived agonist of Dectin-2 (13), ManLAM is required for maximal lipid droplet accumulation during infection, and that ManLAM-induced lipid droplets mirror those elicited by live bacilli in triglyceride composition and dependence on the mTORC1-PPARγ axis. Collectively, these results connect ManLAM architecture with dual receptor recognition and macrophage lipid metabolic reprogramming during infection, establishing coordinated innate receptor engagement as a mechanistic basis for foam cell formation in TB.

Our findings establish a generalizable and previously unrecognized principle in host receptor–microbial ligand interactions, that a single ligand can integrate multiple host sensing mechanisms. Innate immune recognition has traditionally been viewed as individual receptors binding to cognate ligands, with signal integration occurring downstream through pathway crosstalk. Although co-activation of multiple pattern-recognition receptors -- often termed receptor crosstalk – is now recognized as an important determinant of inflammatory responses, relatively little attention has been paid to coordination at the level of ligand recognition itself. For example, cooperative signaling between CLRs and TLRs has been described in the response to fungal infections (46); however, such cooperation is generally attributed to recognition of distinct fungal components by different receptors. In contrast, our work demonstrates that a single microbial factor can engage multiple distinct pattern-recognition receptors through chemically distinct moieties within the same molecule, thereby placing ligands for Dectin-2 and TLR2 in

close molecular proximity. Prior work has shown that productive crosstalk between Dectin-1 and TLR2 depends on spatial coordination of their independent ligands (47, 48). By analogy, expression of ligands for two receptors within one molecule (or molecule family) may facilitate integration of parallel signaling cascades while preserving modular control, promoting synergy even when individual receptor–ligand interactions are of low affinity. Such ligand-level coordination may represent a strategy by which microbes with complex, lipoglycan-rich cell envelopes, such as mycobacteria and fungi, orchestrate integrated host responses.

Our work raises mechanistic considerations regarding how ManLAM-driven inflammatory and lipogenic programs are integrated in macrophages. Our data reveal synergistic activation of both lipid droplet accumulation and NF-κB signaling following co-engagement of TLR2 and Dectin-2 by ManLAM. Notably, however, these outputs are largely independent: inhibition of NF-κB in ManLAM-treated macrophages neither reduces lipid droplet accumulation nor impairs PPARγ activity, which is required for neutral lipid storage. This functional dissociation is consistent with prior observations in *M. tuberculosis*-infected macrophages (26, 45) and indicates that, despite canonical coupling of TLR and CLR signaling to NF-κB activation, lipid droplet biogenesis is not governed primarily by NF-κB-dependent inflammatory signaling**.** This interpretation is supported by established signaling biology. In addition to activating NF-κB (34), TLR2 and Dectin-2 can independently engage the mTORC1-PPARγ axis at multiple levels, including via PI3K/Akt signaling downstream of MyD88 or Syk, respectively (49, 50). Together, these findings support a model in which ManLAM-induced lipid metabolic reprogramming and inflammatory signaling are concurrently engaged yet mechanistically separable. At the same time, the pronounced synergy observed upon dual TLR2 and Dectin-2 engagement by ManLAM in both lipid metabolic reprogramming and inflammatory signaling suggests convergence at shared upstream regulatory nodes. One such candidate is the PI3K/Akt axis, which lies upstream of both NF-κB and mTORC1-PPARγ signaling (51). Thus, ManLAM may promote robust foam cell formation by activating parallel signaling pathways that converge on common control points, providing both mechanistic resilience and potential targets for therapeutic intervention.

Our findings further show that the lipid-inducing activity of ManLAM closely mirrors, but does not fully recapitulate, that elicited by live *M. tuberculosis*. As observed during infection (26), ManLAM drives the accumulation of triglyceride-rich lipid droplets in macrophages through a process that depends on mTORC1 and PPARγ and is only modestly, if at all, sensitive to NF-κB

inhibition. Lipid droplet accumulation during *M. tuberculosis* infection is reduced in Dectin-2- or TLR2-deficient macrophages, consistent with a role for ManLAM in vivo, particularly given that it is the only known *M. tuberculosis*–derived agonist of Dectin-2 (13). Notably, whereas TLR2 or Dectin-2 deficiency fully abrogates ManLAM-induced lipid droplet formation, it only partially attenuates lipid accumulation during infection, indicating that ManLAM contributes substantially but not exclusively to foam cell formation. Additional microbial and host-derived inputs -- including trehalose dimycolate and mycolic acids (52, 53), cGAS–STING activation (54), and autocrine or paracrine TNF signaling (26) -- likely cooperate in this process. Together, these observations support a hierarchical model in which ManLAM-dependent surface receptor signaling acts as an upstream driver of lipid metabolic reprogramming, while additional pathways modulate the magnitude and persistence of foam cell formation across stages of infection. Importantly, convergence on shared downstream regulators, including mTORC1 and PPARγ, defines actionable nodal control points through which pathogenic foam cell formation may be disrupted despite upstream signaling redundancy.

These mechanistic insights have therapeutic implications. Current antibiotic regimens remain inadequate because *M. tuberculosis* is intrinsically insensitive to many antibiotics, enters drug-tolerant states, and continues to evolve antibiotic resistance (55). There is growing consensus that host-directed therapies can enhance antibiotic efficacy and help limit the emergence of antibiotic resistance (56). Because foam cells drive pathology in diverse conditions (4), they have emerged as attractive targets for therapeutic intervention, as exemplified by atherosclerosis (57). By defining how inflammatory and metabolic signaling pathways are integrated during foam cell biogenesis in TB, our work provides a framework for identifying host-directed therapeutic strategies**,** with potential relevance not only to TB but also to other diseases characterized by pathogenic foam cell formation.

Acknowledgements

We thank Karl Drlica for critical comments on the manuscript, and staff of the Flow Cytometry and Immunology Core Laboratory at Rutgers New Jersey Medical School for assistance with imaging flow cytometry. This work was funded in part by AHA fellowship 24PRE1198252 (J.R.), NIH grants R01HL149450, R01AI158911, NCATS UM1TR004789 (M.L.G.), R35GM124918 (Y. Y.), NIH DP2AI154429 (S.B.), and a grant from the Fondation pour la Recherche Médicale Equipes FRM DEQ20180339208 (J.N.).

Author contributions

D.N., M.G., S.B., J.N., and Y.Y. contributed to the experimental design; D.N., J.R., O.V., S.B., J.C., and J.N. performed experiments and analyzed data; D.N. and M.G. wrote the manuscript. All authors reviewed and edited the manuscript.

References

1. WorldHealthOrganization (2025) Global tuberculosis report. (World Health Organization, Geneva, Switzerland).
2. J. L. Flynn, J. Chan, P. L. Lin, Macrophages and control of granulomatous inflammation in tuberculosis. *Mucosal Immunology* **4**, 271-278 (2011).
3. L. Ramakrishnan, Revisiting the role of the granuloma in tuberculosis. *Nat Rev Immunol* **12**, 352-366 (2012).
4. V. Guerrini, M. L. Gennaro, Foam Cells: One Size Doesn't Fit All. *Trends Immunol* **40**, 1163-1179 (2019).
5. P. Peyron *et al.*, Foamy macrophages from tuberculous patients' granulomas constitute a nutrient-rich reservoir for M. tuberculosis persistence. *PLoS Pathog* **4**, e1000204 (2008).
6. D. J. Greenwood *et al.*, Subcellular antibiotic visualization reveals a dynamic drug reservoir in infected macrophages. *Science* **364**, 1279-1282 (2019).
7. J. Nigou, M. Gilleron, G. Puzo, Lipoarabinomannans: from structure to biosynthesis. *Biochimie* **85**, 153-166 (2003).
8. A. K. Mishra, N. N. Driessen, B. J. Appelmelk, G. S. Besra, Lipoarabinomannan and related glycoconjugates: structure, biogenesis and role in Mycobacterium tuberculosis physiology and host-pathogen interaction. *FEMS Microbiol Rev* **35**, 1126-1157 (2011).
9. J. B. Torrelles, D. Chatterjee, Collected Thoughts on Mycobacterial Lipoarabinomannan, a Cell Envelope Lipoglycan. *Pathogens* **12** (2023).
10. I. L. Sparks *et al.*, Lipoarabinomannan mediates localized cell wall integrity during division in mycobacteria. *Nat Commun* **15**, 2191 (2024).
11. J. Turner, J. B. Torrelles, Mannose-capped lipoarabinomannan in Mycobacterium tuberculosis pathogenesis. *Pathog Dis* **76** (2018).
12. I. Vergne, M. Gilleron, J. Nigou, Manipulation of the endocytic pathway and phagocyte functions by Mycobacterium tuberculosis lipoarabinomannan. *Front Cell Infect Microbiol* **4**, 187 (2014).
13. A. Decout *et al.*, Deciphering the molecular basis of mycobacteria and lipoglycan recognition by the C-type lectin Dectin-2. *Sci Rep* **8**, 16840 (2018).
14. A. Yonekawa *et al.*, Dectin-2 is a direct receptor for mannose-capped lipoarabinomannan of mycobacteria. *Immunity* **41**, 402-413 (2014).
15. J. Nigou *et al.*, Mannan chain length controls lipoglycans signaling via and binding to TLR2. *J Immunol* **180**, 6696-6702 (2008).

16. A. Ray, M. Cot, G. Puzo, M. Gilleron, J. Nigou, Bacterial cell wall macroamphiphiles: pathogen-/microbe-associated molecular patterns detected by mammalian innate immune system. *Biochimie* **95**, 33-42 (2013).
17. H. D'Avila *et al.*, Mycobacterium bovis bacillus Calmette-Guerin induces TLR2-mediated formation of lipid bodies: intracellular domains for eicosanoid synthesis in vivo. *J Immunol* **176**, 3087-3097 (2006).
18. P. E. Almeida *et al.*, Mycobacterium bovis bacillus Calmette-Guerin infection induces TLR2-dependent peroxisome proliferator-activated receptor gamma expression and activation: functions in inflammation, lipid metabolism, and pathogenesis. *J Immunol* **183**, 1337-1345 (2009).
19. U. Zahringer, B. Lindner, S. Inamura, H. Heine, C. Alexander, TLR2 - promiscuous or specific? A critical re-evaluation of a receptor expressing apparent broad specificity. *Immunobiology* **213**, 205-224 (2008).
20. S. Xie, J. Duan, B. Li, P. Zhou, G. C. Hon, Multiplexed Engineering and Analysis of Combinatorial Enhancer Activity in Single Cells. *Mol Cell* **66**, 285-299.e285 (2017).
21. J. G. Doench *et al.*, Optimized sgRNA design to maximize activity and minimize off-target effects of CRISPR-Cas9. *Nature Biotechnology* **34**, 184-191 (2016).
22. K. R. Sanson *et al.*, Optimized libraries for CRISPR-Cas9 genetic screens with multiple modalities. *Nature Communications* **9**, 5416 (2018).
23. C. Vilcheze *et al.*, Rational Design of Biosafety Level 2-Approved, Multidrug-Resistant Strains of Mycobacterium tuberculosis through Nutrient Auxotrophy. *mBio* **9** (2018).
24. S. L. Bell, K. L. Lopez, J. S. Cox, K. L. Patrick, R. O. Watson, Galectin-8 Senses Phagosomal Damage and Recruits Selective Autophagy Adapter TAX1BP1 To Control Mycobacterium tuberculosis Infection in Macrophages. *mBio* **12**, e0187120 (2021).
25. R. O. Watson *et al.*, The Cytosolic Sensor cGAS Detects Mycobacterium tuberculosis DNA to Induce Type I Interferons and Activate Autophagy. *Cell Host Microbe* **17**, 811-819 (2015).
26. V. Guerrini *et al.*, Storage lipid studies in tuberculosis reveal that foam cell biogenesis is disease-specific. *PLoS Pathog* **14**, e1007223 (2018).
27. H. M. Shin *et al.*, Inhibitory action of novel aromatic diamine compound on lipopolysaccharide-induced nuclear translocation of NF-kappaB without affecting IkappaB degradation. *FEBS Lett* **571**, 50-54 (2004).

28. S. Strickson *et al.*, The anti-inflammatory drug BAY 11-7082 suppresses the MyD88-dependent signalling network by targeting the ubiquitin system. *Biochem J* **451**, 427-437 (2013).
29. S. Shukla, E. T. Richardson, M. G. Drage, W. H. Boom, C. V. Harding, Mycobacterium tuberculosis Lipoprotein and Lipoglycan Binding to Toll-Like Receptor 2 Correlates with Agonist Activity and Functional Outcomes. *Infect Immun* **86** (2018).
30. S. Krishna *et al.*, Lipoglycans contribute to innate immune detection of mycobacteria. *PLoS One* **6**, e28476 (2011).
31. I. Spera *et al.*, The J2-Immortalized Murine Macrophage Cell Line Displays Phenotypical and Metabolic Features of Primary BMDMs in Their M1 and M2 Polarization State. *Cancers (Basel)* **13** (2021).
32. K. Sato *et al.*, Dectin-2 is a pattern recognition receptor for fungi that couples with the Fc receptor gamma chain to induce innate immune responses. *J Biol Chem* **281**, 38854-38866 (2006).
33. M. Gilleron, J. Nigou, D. Nicolle, V. Quesniaux, G. Puzo, The acylation state of mycobacterial lipomannans modulates innate immunity response through toll-like receptor 2. *Chem Biol* **13**, 39-47 (2006).
34. T. Liu, L. Zhang, D. Joo, S.-C. Sun, NF-κB signaling in inflammation. *Signal Transduction and Targeted Therapy* **2**, 17023 (2017).
35. M. S. Hayden, S. Ghosh, Shared Principles in NF-κB Signaling. *Cell* **132**, 344-362 (2008).
36. W. Li, M. Li, S. M. Anthony, Y. Yu, Spatial organization of FcγR and TLR2/1 on phagosome membranes differentially regulates their synergistic and inhibitory receptor crosstalk. *Scientific Reports* **11**, 13430 (2021).
37. H. Salamon *et al.*, Cutting Edge: Vitamin D Regulates Lipid Metabolism in Mycobacterium tuberculosis Infection. *J Immunol* 10.4049/jimmunol.1400736 (2014).
38. M. Laplante, D. M. Sabatini, Regulation of mTORC1 and its impact on gene expression at a glance. *J Cell Sci* **126**, 1713-1719 (2013).
39. S. J. Ricoult, B. D. Manning, The multifaceted role of mTORC1 in the control of lipid metabolism. *EMBO Rep* **14**, 242-251 (2013).
40. M. Angela *et al.*, Fatty acid metabolic reprogramming via mTOR-mediated inductions of PPARgamma directs early activation of T cells. *Nat Commun* **7**, 13683 (2016).

41. N. Arimura, T. Horiba, M. Imagawa, M. Shimizu, R. Sato, The Peroxisome Proliferator-activated Receptor γ Regulates Expression of the Perilipin Gene in Adipocytes *. *Journal of Biological Chemistry* **279**, 10070-10076 (2004).
42. J. P. Cogswell *et al.*, NF-kappa B regulates IL-1 beta transcription through a consensus NF-kappa B binding site and a nonconsensus CRE-like site. *J Immunol* **153**, 712-723 (1994).
43. S. C. Land, A. R. Tee, Hypoxia-inducible Factor 1α Is Regulated by the Mammalian Target of Rapamycin (mTOR) via an mTOR Signaling Motif*. *Journal of Biological Chemistry* **282**, 20534-20543 (2007).
44. P. van Uden, N. S. Kenneth, S. Rocha, Regulation of hypoxia-inducible factor-1alpha by NF-kappaB. *Biochem J* **412**, 477-484 (2008).
45. M. V. Rajaram *et al.*, Mycobacterium tuberculosis activates human macrophage peroxisome proliferator-activated receptor gamma linking mannose receptor recognition to regulation of immune responses. *J Immunol* **185**, 929-942 (2010).
46. A. Plato, S. E. Hardison, G. D. Brown, Pattern recognition receptors in antifungal immunity. *Semin Immunopathol* **37**, 97-106 (2015).
47. W. Li, J. Yan, Y. Yu, Geometrical reorganization of Dectin-1 and TLR2 on single phagosomes alters their synergistic immune signaling. *Proceedings of the National Academy of Sciences* **116**, 25106-25114 (2019).
48. M. Li, C. Vultorius, M. Bethi, Y. Yu, Spatial Organization of Dectin-1 and TLR2 during Synergistic Crosstalk Revealed by Super-resolution Imaging. *The Journal of Physical Chemistry B* **126**, 5781-5792 (2022).
49. M. H. Laird *et al.*, TLR4/MyD88/PI3K interactions regulate TLR4 signaling. *J Leukoc Biol* **85**, 966-977 (2009).
50. O. Hatton *et al.*, Syk activation of phosphatidylinositol 3-kinase/Akt prevents HtrA2-dependent loss of X-linked inhibitor of apoptosis protein (XIAP) to promote survival of Epstein-Barr virus+ (EBV+) B cell lymphomas. *J Biol Chem* **286**, 37368-37378 (2011).
51. B. D. Manning, L. C. Cantley, AKT/PKB signaling: navigating downstream. *Cell* **129**, 1261-1274 (2007).
52. M. J. Kim *et al.*, Caseation of human tuberculosis granulomas correlates with elevated host lipid metabolism. *EMBO Mol Med* **2**, 258-274 (2010).
53. H. K. Dkhar *et al.*, Mycobacterium tuberculosis keto-mycolic acid and macrophage nuclear receptor TR4 modulate foamy biogenesis in granulomas: a case of a heterologous and noncanonical ligand-receptor pair. *J Immunol* **193**, 295-305 (2014).

54. S. Liu *et al.*, Mycobacterium tuberculosis suppresses host DNA repair to boost its intracellular survival. *Cell Host Microbe* **31**, 1820-1836 e1810 (2023).

55. R. M. Jones, K. N. Adams, H. E. Eldesouky, D. R. Sherman, The evolving biology of Mycobacterium tuberculosis drug resistance. *Front Cell Infect Microbiol* **12**, 1027394 (2022).

56. S. Krug, S. Parveen, W. R. Bishai, Host-Directed Therapies: Modulating Inflammation to Treat Tuberculosis. *Front Immunol* **12**, 660916 (2021).

57. A. C. Li, C. K. Glass, The macrophage foam cell as a target for therapeutic intervention. *Nat Med* **8**, 1235-1242 (2002).

Figure legends

Figure 1: Involvement of TLR2 signaling in lipid droplet induction by *M. tuberculosis* lipoarabinomannan. A. *M. tuberculosis* ManLAM (500 ng/ml), H_2O_2-treated ManLAM (ML+H; 500 ng/ml), Pam3CSK4 (PAM, synthetic TLR2 agonist; 500 ng/ml) and vehicle control (C) were tested for ability to induce NF-κB activation in HEK-TLR2 reporter cells. Reporter cells were treated for 24h and TLR2 activity was measured as a function of inducible secreted embryonic alkaline phosphatase in a colorimetric assay at 650nm. The ratio of OD at 650nm of treated vs. vehicle-treated cells were plotted in the Y-axis. **B.** CRISPRi technology was used to generate TLR2 knock-down (KD) murine iBMDM. Control (non-targeting guide RNAs) and TLR2 KD clones were treated for 24h with 500ng/ml ManLAM preparations and Pam3CSK4. Abbreviations are as in panel A. Macrophages were stained with Bodipy 493/503 and antibodies to the macrophage marker F4/80. Data were obtained by imaging flow cytometry in triplicate and expressed as ratio of Bodipy mean fluorescence intensity (MFI) of treated vs. vehicle-treated cells. The horizontal dotted line marks the vehicle-treated cell reading. Comparison for statistical significance was between treated and vehicle-treated cells. **C**. Representative microscopy images (60x magnification) of vehicle-control (C) and treated iBMDM in the experiment shown in panel B. Fluorescence stain: Bodipy 493/503 (neutral lipid dye, green fluorescence). **D.** iBMDM were treated with ManLAM (500 ng/ml) and increasing doses of Pam3CSK4 (10, 50, 100, 500 ng/ml) for 24h. Data were generated and expressed as in panel B. **E.** Representative images (60x magnification) of the experiment shown in panel D. Description of the images as in panel C. *, p <0.05 by unpaired t test in all relevant panels.

Figure 2: Involvement of Dectin-2 signaling in lipid droplet induction by *M. tuberculosis* lipoarabinomannan. A. *M. tuberculosis* ManLAM (500 ng/ml), H_2O_2 treated ManLAM (ML+H, 500 ng/ml), furfurman (FUR; commercial Dectin-2 agonist; 10 µg/ml) and vehicle control (C) were tested were tested for ability to induce NF-κB activation in HEK-Dectin-2 reporter cells. Data were generated and analyzed as in Fig. 1A. **B.** Control and Dectin-2 knockdown (KD) iBMDM were treated 24h with 500ng/ml ManLAM preparations. Abbreviations are as in panel A. Imaging flow cytometry data were generated and expressed as in Fig. 1B. **C.** Representative microscopy images (60x magnification) of vehicle-control (C) and treated iBMDM in the experiment shown in panel B. Panel description as in Fig. 1C. **D.** iBMDM were treated with ManLAM (500 ng/ml) doses of furfurman (FUR; 2.5, 5 and 10 µg/ml). Imaging flow cytometry data were generated and expressed as in Fig. 1B. **E.** Representative microscopy images (60x

magnification) of vehicle-control (C) and treated iBMDM in the experiment shown in panel D. Panel description as in Fig. 1C. *, p <0.05 by unpaired t test in all relevant panels.

Figure 3: Involvement of *M. tuberculosis* lipoarabinomannan moieties in lipid droplet induction. A. iBMDM were treated with Pam3CSK4 (PAM; 500 ng/ml) and furfurman (FUR; 10 µg/ml), singly or in combination (PAM+FUR), and corresponding vehicle controls. Imaging flow cytometry data were generated and expressed as in Fig. 1B. **B.** Representative microscopy images (60x magnification) of vehicle-control (C) and treated iBMDM in the experiment shown in panel A. Panel description as in Fig. 1C. **C.** *M. tuberculosis* ManLAM, demannosylated ManLAM (αtManLAM), and deacylated ManLAM (dManLAM) (all H_2O_2 pre-treated, 500 ng/ml) and corresponding vehicle controls were tested for ability to induce NF-κB activation in HEK-TLR2 and HEK-Dectin 2 reporter cells. Treatment was for 24h as in preceding figures. Data are presented as ratio of OD_{650} values obtained with treated vs vehicle control cells. The horizontal dotted line marks the corresponding vehicle-control reading. **D.** ManLAM and derivatives, as in panel C, were used to treat iBMDM (all 500 ng/ml for 24h). Imaging flow cytometry data were generated and expressed as in Fig. 1B. **E.** Representative microscopy images (60x magnification) of vehicle-control (C) and treated iBMDM in the experiment shown in panel D. Panel description as in Fig. 1C. *, p <0.05 by unpaired t test in all relevant panels.

Figure 4: Ligand-dependent NF-κB RelA nuclear translocation dynamics in EGFP-RelA RAW264.7 macrophages. **A.** Schematic illustrating cytoplasm-to-nucleus translocation of NF-kκB RelA (p65) upon macrophage cell stimulation. Grey circles, ManLAM and derivatives; red rods, RelA. **B.** (Top row) Time-lapse live-cell epifluorescence images showing EGFP-RelA translocation following ManLAM stimulation. (Bottom row) Same cell images shown with EGFP-RelA fluorescence intensity encoded in pseudo-color, as indicated by the color bar. Scale bars: 5 µm. **C.** Quantification of RelA nuclear translocation over time for the representative cell shown in panel B and for an unstimulated control cell, expressed as the fluorescence intensity ratio of EGFP-RelA in the nucleus relative to the cytoplasm. **D.** Representative epifluorescence images of fixed EGFP-RelA RAW264.7 macrophages stimulated with *M. tuberculosis* ManLAM, demannosylated ManLAM (αtManLAM), and deacylated ManLAM (dManLAM) or furfurman (FUR) for 240 min, or with Pam3CSK4 for 60 min, illustrating ligand-induced RelA nuclear translocation. Scale bars: 10 µm. **E.** Percentage of responsive and non-responsive cells under

various ligand stimulation conditions, as indicated. Responsive cells were defined as those with a RelA nucleus-to-cytosol ratio greater than 1.089, a threshold set to achieve 95% of unstimulated cells being classified as non-responsive**.** Approximately 200 cells per condition were analyzed; the fraction of responsive cells was 40% for ManLAM, 21% for αtManLAM, 16% for dManLAM, 28% for furfurman (FUR), and 80% for Pam3CSK4. **F.** Single-cell scatter plots of NF-κB activation, expressed as the nucleus-to-cytosol EGFP-RelA fluorescence intensity ratio, in all responsive cells after 240 min ligand stimulation (for ManLAM and derivatives, and furfurman) and 60 min for Pam3CSK4. Each dot represents one cell. Box plots show the interquartile range and the median line; whiskers indicate ±1.5× SD. Statistical significance was assessed by one-way ANOVA: ***P < 0.001; **P < 0.01; *P < 0.05.

Figure 5: Effects on lipid droplet content of knocking down TLR2 and Dectin-2 in *M. tuberculosis*-infected macrophages and treatment with neutral lipid biosynthesis inhibitors in lipoarabinomannan-treated macrophages. A. iBMDM, control (C, non-targeting guide RNAs), TLR2 knock-down (KD), and Dectin-2 (Dec-2) KD iBMDM clones were left uninfected or infected with *M. tuberculosis* $mc^2$6206 (MOI= 15) for 48h in triplicate wells, washed, and stained with Bodipy 493/503 and antibodies to the macrophage marker F4/80 for imaging flow cytometry. Data were generated and expressed as in Fig. 1B. **B.** Representative microscopy images (60x magnification) of uninfected (U) and infected (Mtb) iBMDM in the experiment shown in panel A. Panel description as in Fig. 1C. **C, D.** iBMDM were treated with ManLAM (500ng/ml) and vehicle-treated or treated with increasing doses of the diacylglycerol transferase inhibitor, A922500 (DGAT-i; 60, 90, 120ng/ml) and the acyl-coenzyme A:cholesterol acyltransferase inhibitor, CAS 615264-52-3 (ACAT-i; 5, 10, 15µg/ml). Imaging flow cytometry data for lipid droplet content were generated and expressed as in Fig. 1B. *, p <0.05 by unpaired t test in all relevant panels. **E.** iBMDM were treated with ManLAM (500ng/ml) and vehicle-treated or treated with increasing doses of the PPARγ inhibitor GW9662 (0.5, 1, 2µM), mTORC1 inhibitor rapamycin (0.2, 0.4, 0.8nM), and the NF-κB inhibitor JSH-23 (3.5, 7, 14µM). Imaging flow cytometry data for lipid droplet content were generated and expressed as in Fig. 1B. *, p <0.05 by unpaired t test in all relevant panels.

Figure 6: ManLAM engages TLR2 and Dectin-2 to drive parallel, mechanistically separable metabolic and inflammatory programs. Acyl groups and mannose caps within

ManLAM engage TLR2 and Dectin-2, respectively, activating an mTORC1-PPARγ pathway that promotes lipid droplet accumulation and an NF-κB pathway that induces inflammatory cytokine production (e.g., TNF-α). Lipid metabolic reprogramming proceeds largely independently of inflammatory signaling.

Figure 1

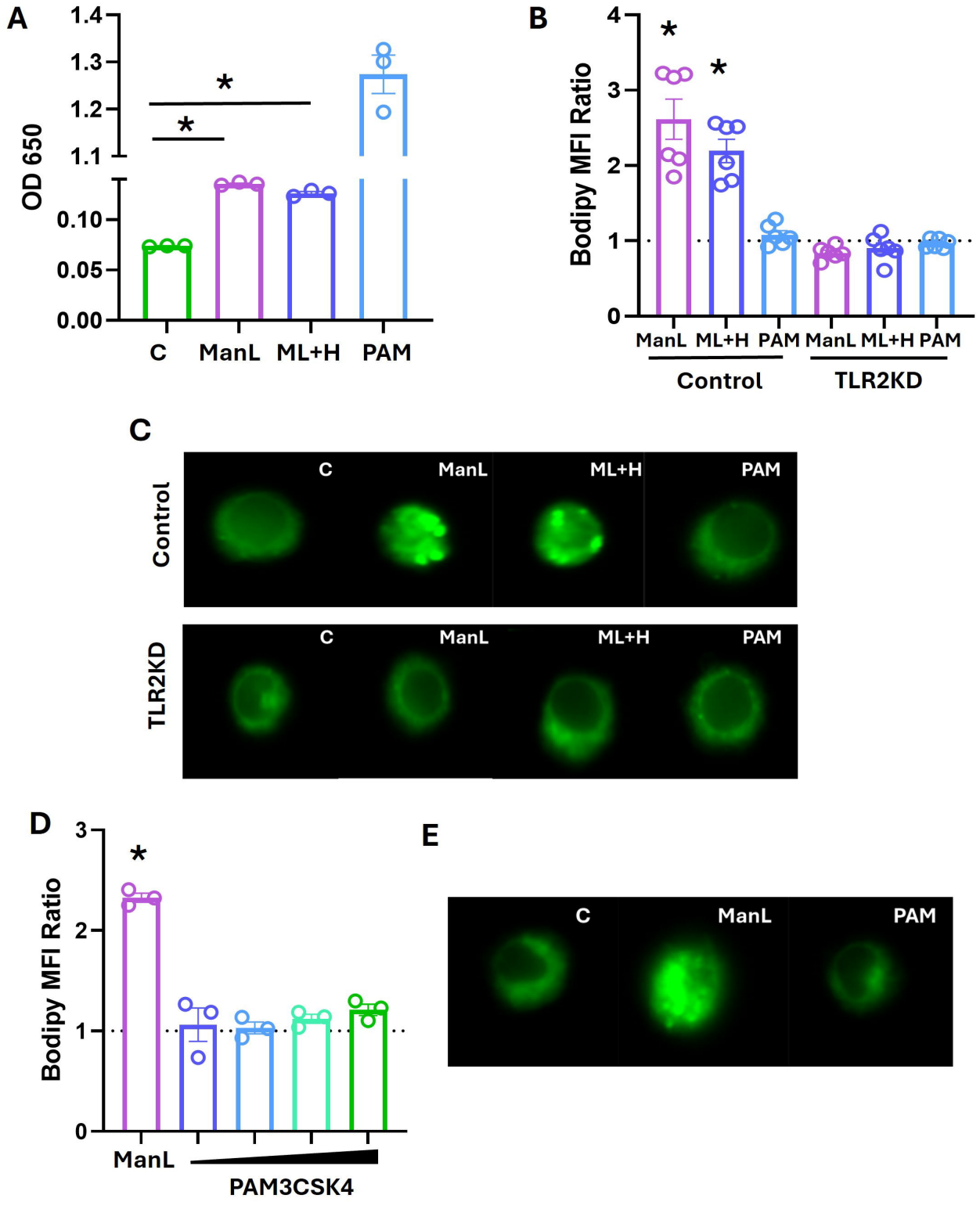
A
OD 650
1.4
1.3
1.2
1.1
0.10
0.05
0.00
*
*
C
ManL
ML+H
PAM
B
Bodipy MFI Ratio
4
3
2
1
0
*
*
ManL
ML+H
PAM
ManL
ML+H
PAM
Control
TLR2KD
C
Control
TLR2KD
C
ManL
ML+H
PAM
C
ManL
ML+H
PAM
D
Bodipy MFI Ratio
3
2
1
0
*
ManL
PAM3CSK4
E
C
ManL
PAM

Figure 2

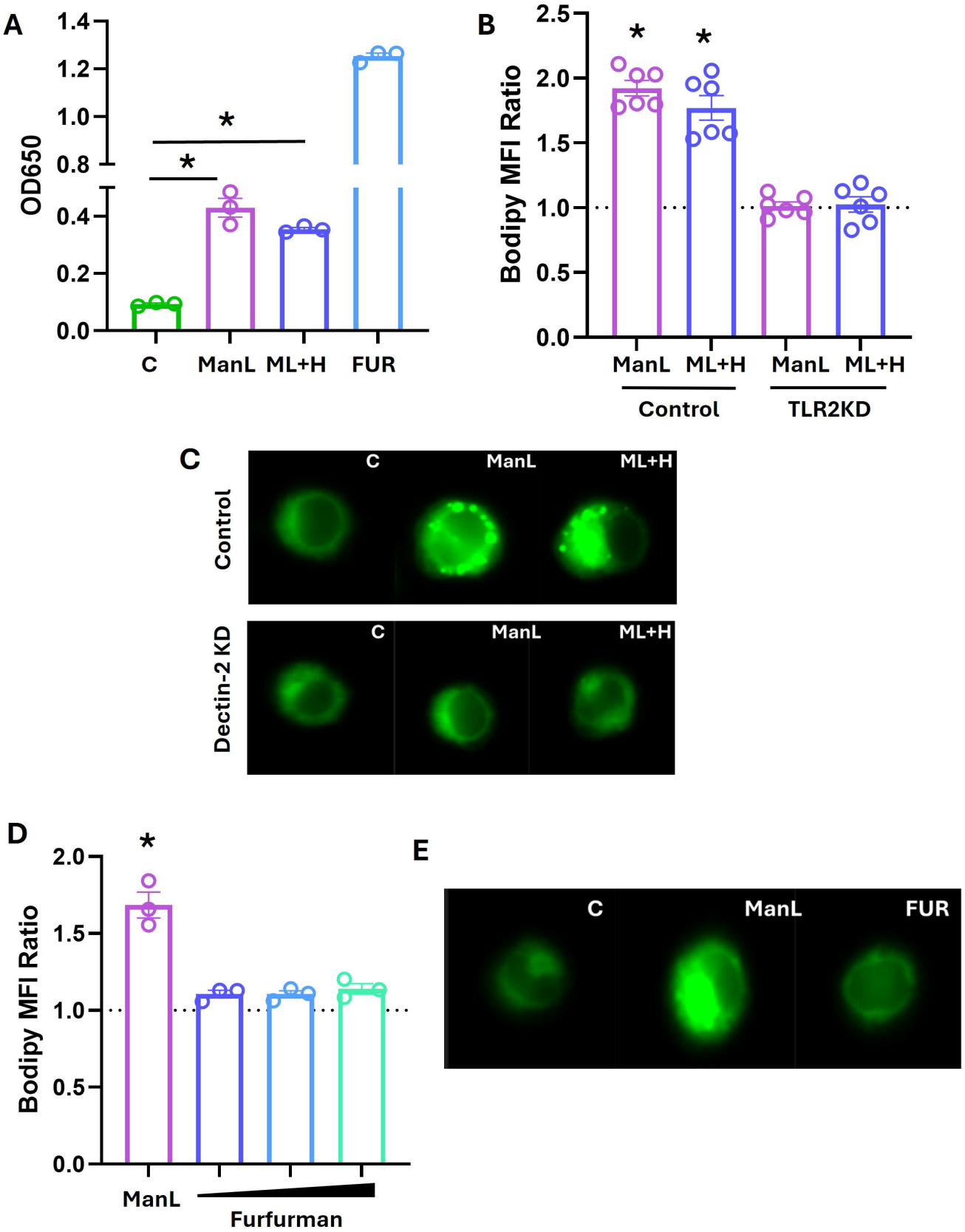
A
OD650
1.4
1.2
1.0
0.8
0.4
0.2
0.0
*
*
C
ManL
ML+H
FUR
B
Bodipy MFI Ratio
2.5
2.0
1.5
1.0
0.5
0.0
*
*
ManL
ML+H
ManL
ML+H
Control
TLR2KD
C
Control
Dectin-2 KD
C
ManL
ML+H
C
ManL
ML+H
D
Bodipy MFI Ratio
2.0
1.5
1.0
0.5
0.0
*
ManL
Furfurman
E
C
ManL
FUR

Figure 3

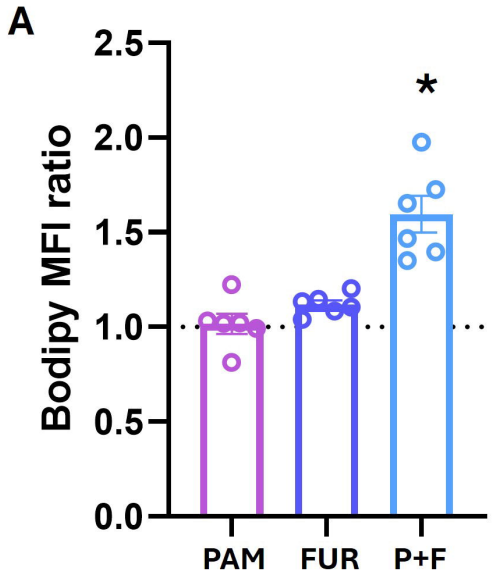
A
Bodipy MFI ratio
2.5
2.0
1.5
1.0
0.5
0.0
*
PAM
FUR
P+F

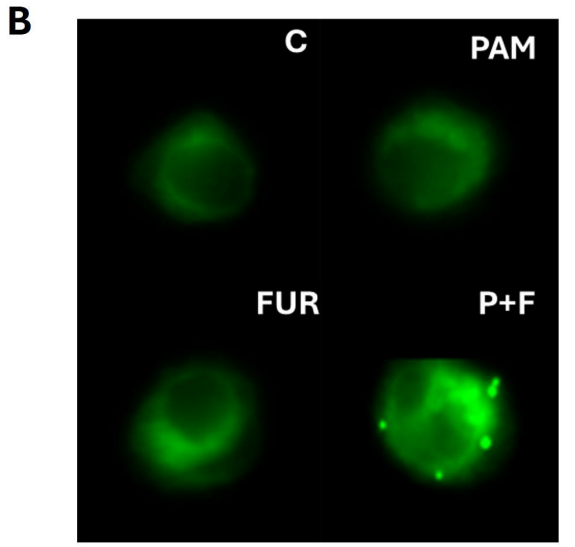
B
C
PAM
FUR
P+F

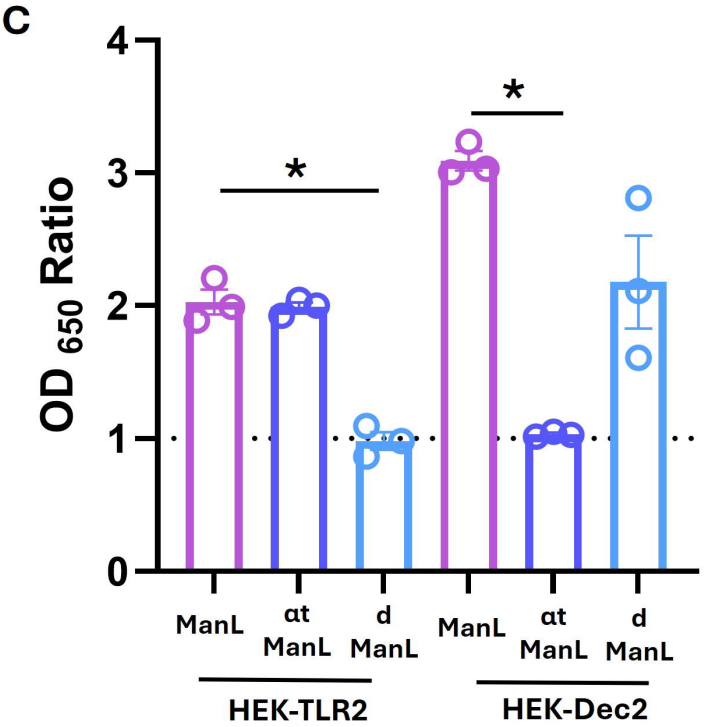
C
OD 650 Ratio
4
3
2
1
0
*
*
ManL
αt ManL
d ManL
ManL
αt ManL
d ManL
HEK-TLR2
HEK-Dec2

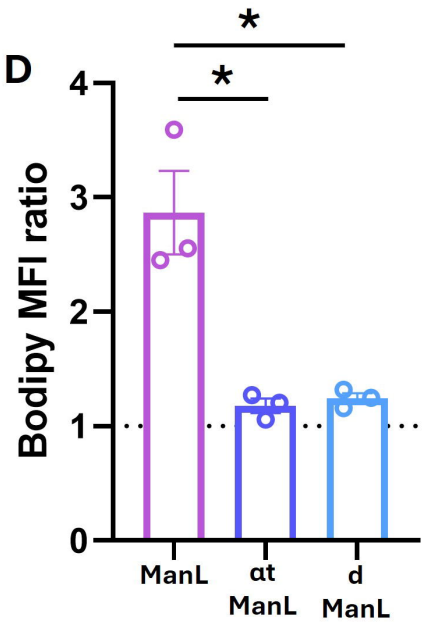
D
Bodipy MFI ratio
4
3
2
1
0
*
*
ManL
αt ManL
d ManL

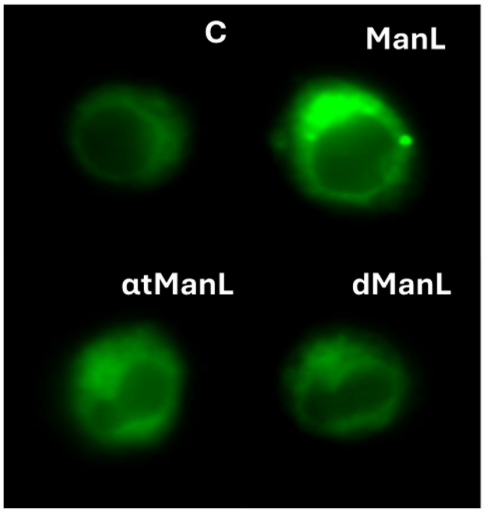
E
C
ManL
αtManL
dManL

Figure 4

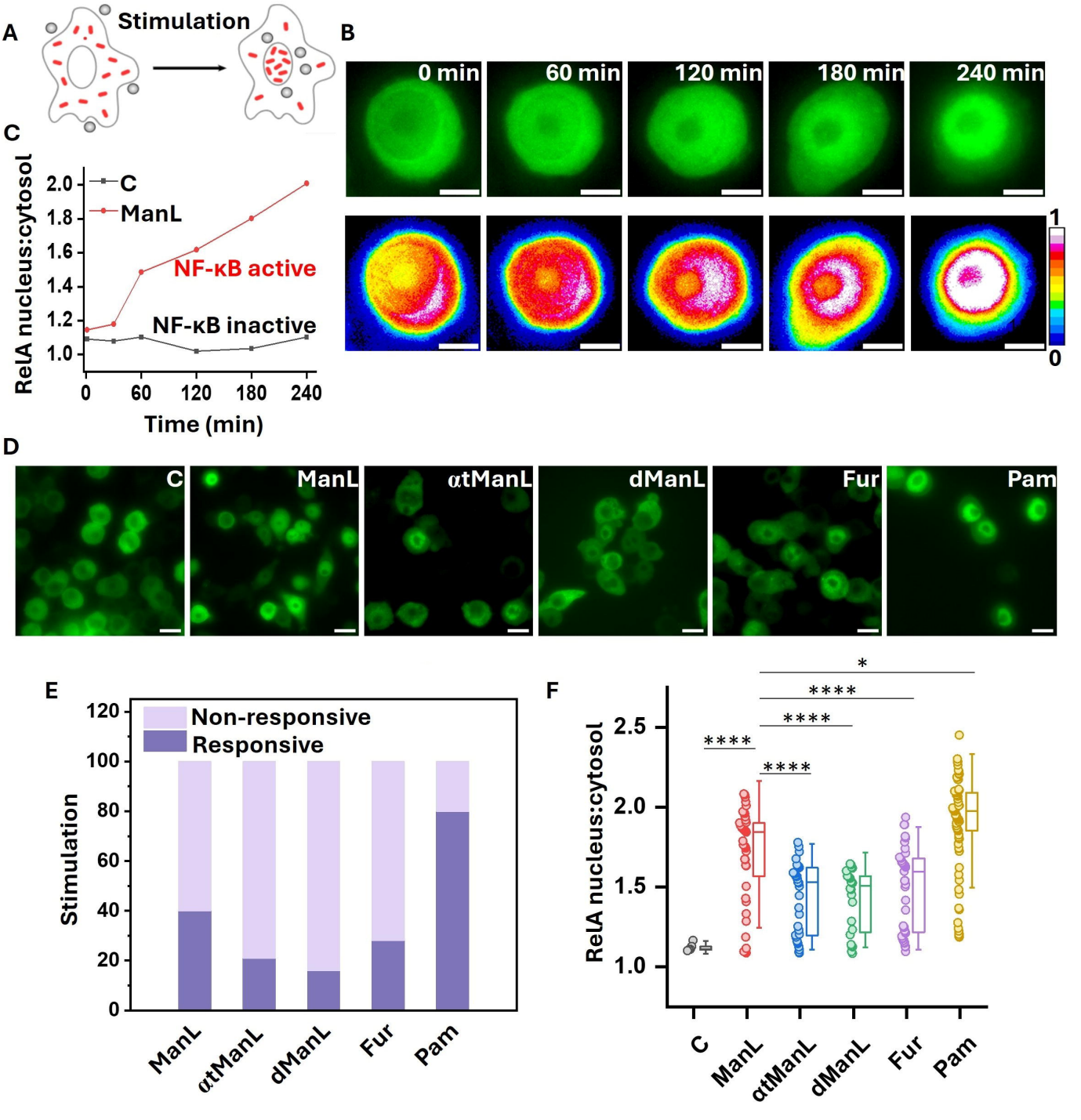
A
Stimulation
B
0 min
60 min
120 min
180 min
240 min
1
0
C
RelA nucleus:cytosol
2.0
1.8
1.6
1.4
1.2
1.0
C
ManL
NF-κB active
NF-κB inactive
0
60
120
180
240
Time (min)
D
C
ManL
αtManL
dManL
Fur
Pam
E
Stimulation
120
100
80
60
40
20
0
Non-responsive
Responsive
ManL
αtManL
dManL
Fur
Pam
F
RelA nucleus:cytosol
2.5
2.0
1.5
1.0
****
****
****
****
*
C
ManL
αtManL
dManL
Fur
Pam

Figure 5

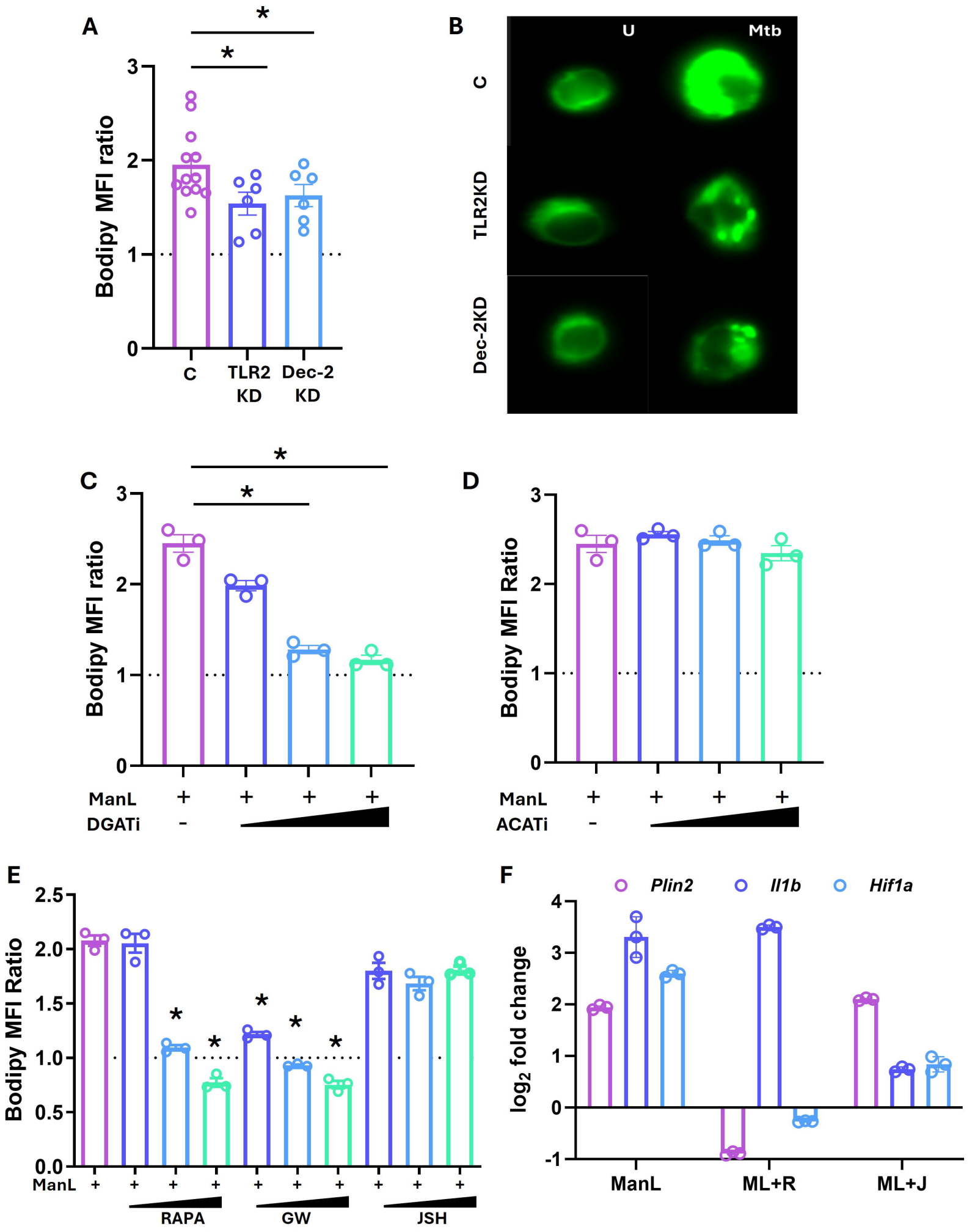
A
Bodipy MFI ratio
C
TLR2 KD
Dec-2 KD
B
U
Mtb
C
TLR2KD
Dec-2KD
C
Bodipy MFI ratio
ManL
DGATi
D
Bodipy MFI Ratio
ManL
ACATi
E
Bodipy MFI Ratio
ManL
RAPA
GW
JSH
F
Plin2
Il1b
Hif1a
log2 fold change
ManL
ML+R
ML+J

Figure 6

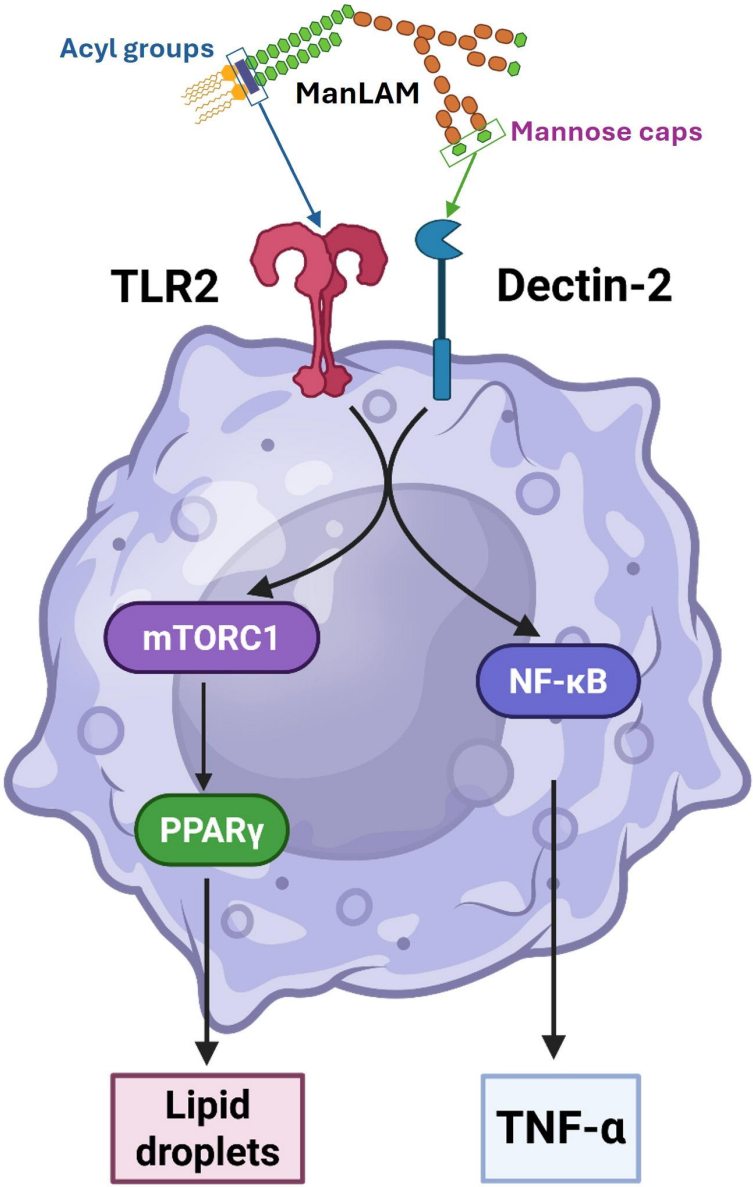
Acyl groups
ManLAM
Mannose caps
TLR2
Dectin-2
mTORC1
NF-κB
PPARγ
Lipid droplets
TNF-α

Figure S1

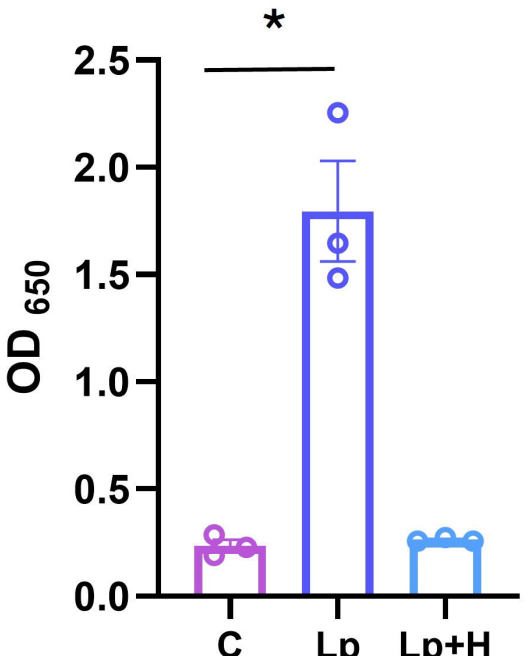

Figure S2

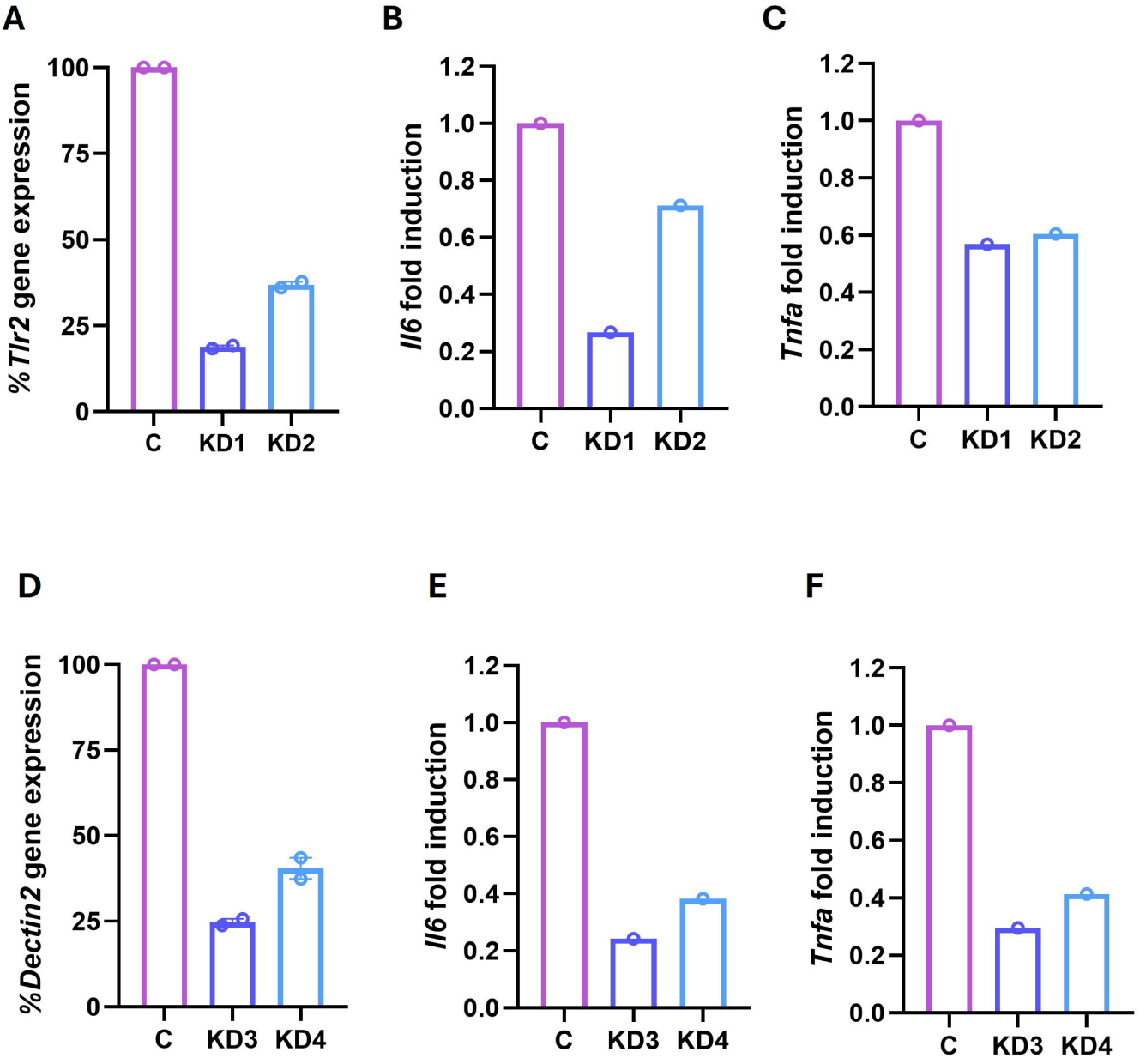
A
% Tlr2 gene expression
100
75
50
25
0
C
KD1
KD2
B
Il6 fold induction
1.2
1.0
0.8
0.6
0.4
0.2
0.0
C
KD1
KD2
C
Tnfa fold induction
1.2
1.0
0.8
0.6
0.4
0.2
0.0
C
KD1
KD2
D
%Dectin2 gene expression
100
75
50
25
0
C
KD3
KD4
E
Il6 fold induction
1.2
1.0
0.8
0.6
0.4
0.2
0.0
C
KD3
KD4
F
Tnfa fold induction
1.2
1.0
0.8
0.6
0.4
0.2
0.0
C
KD3
KD4

Figure S3

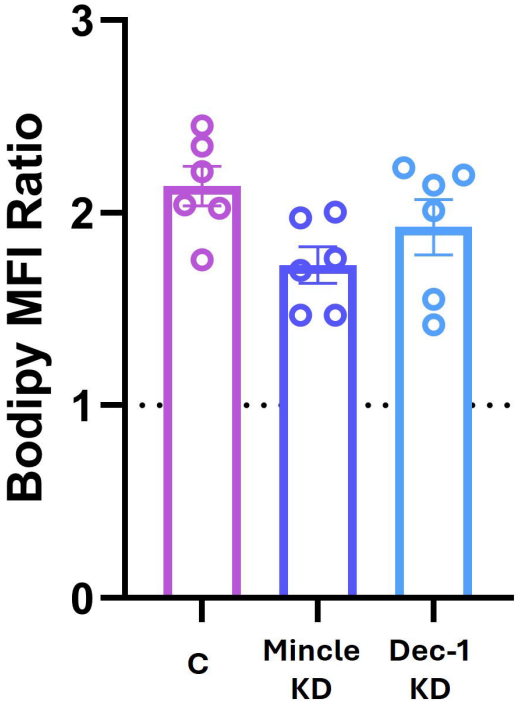

Figure S4

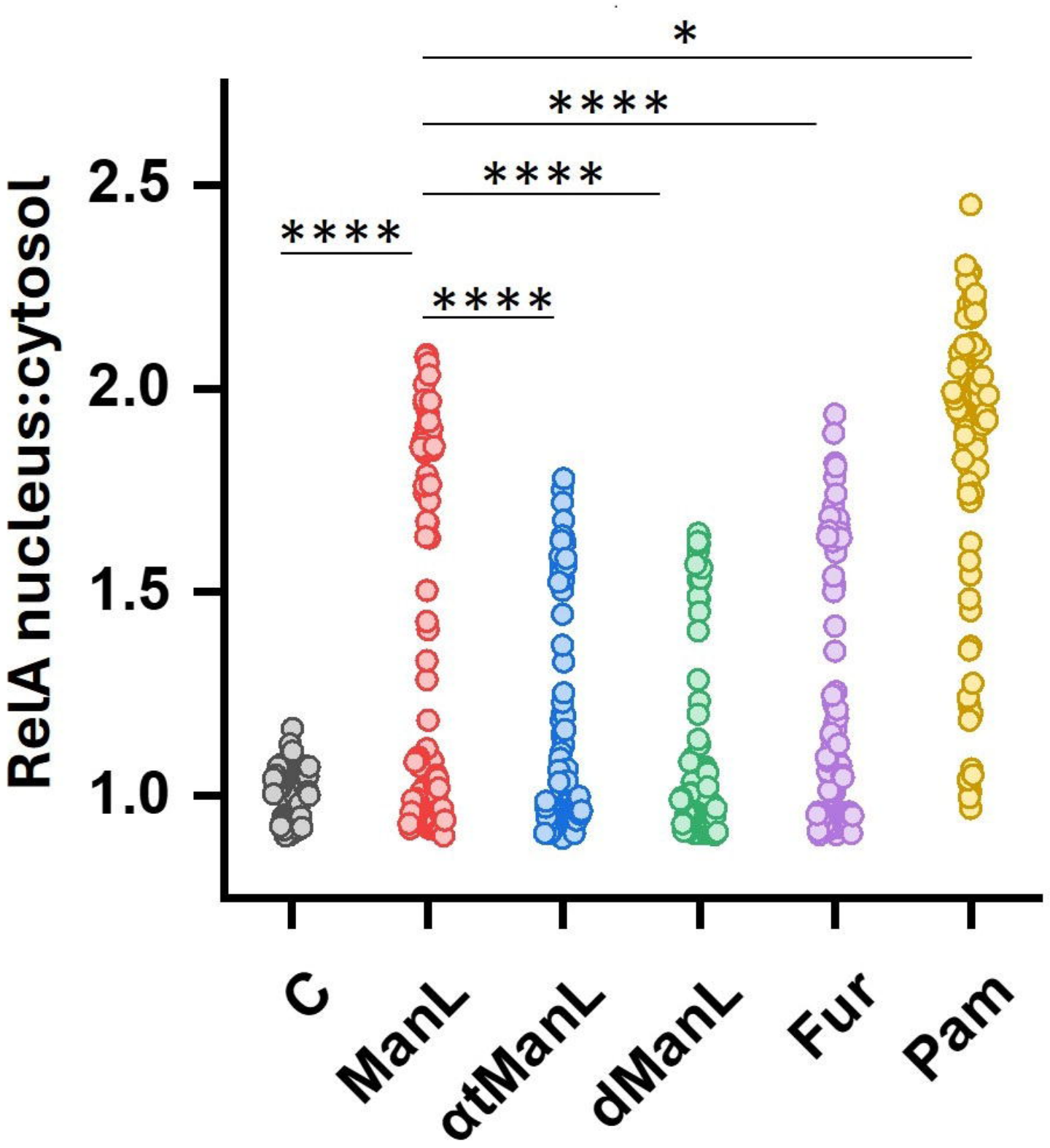

Figure S5

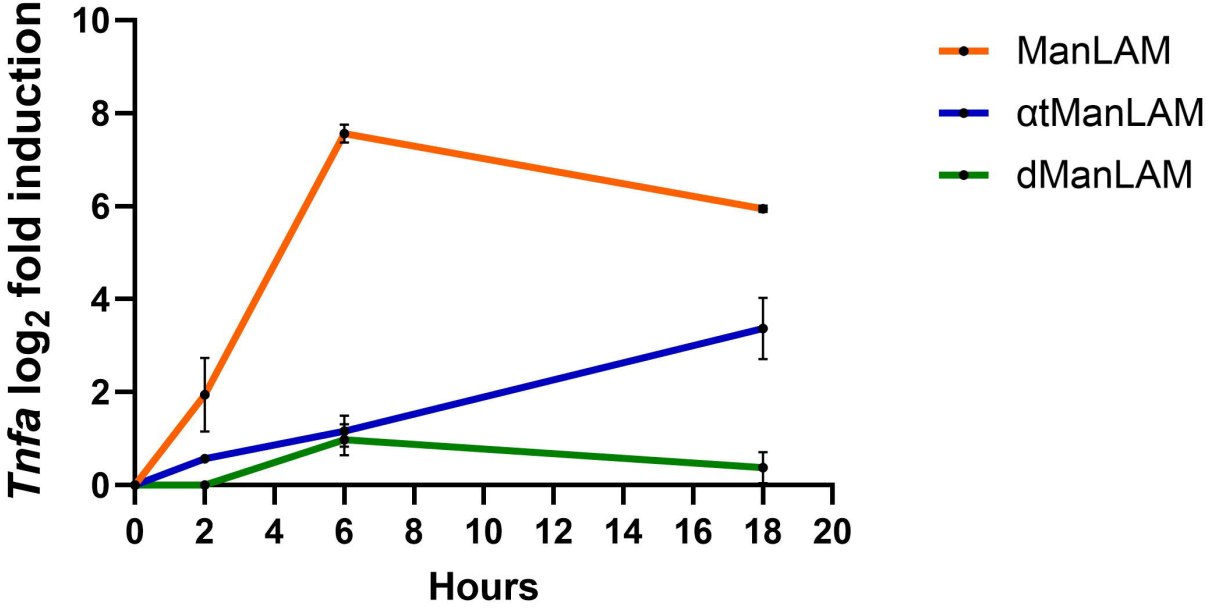
Tnfa $\log_2$ fold induction
10
8
6
4
2
0
0
2
4
6
8
10
12
14
16
18
20
Hours
ManLAM
αtManLAM
dManLAM
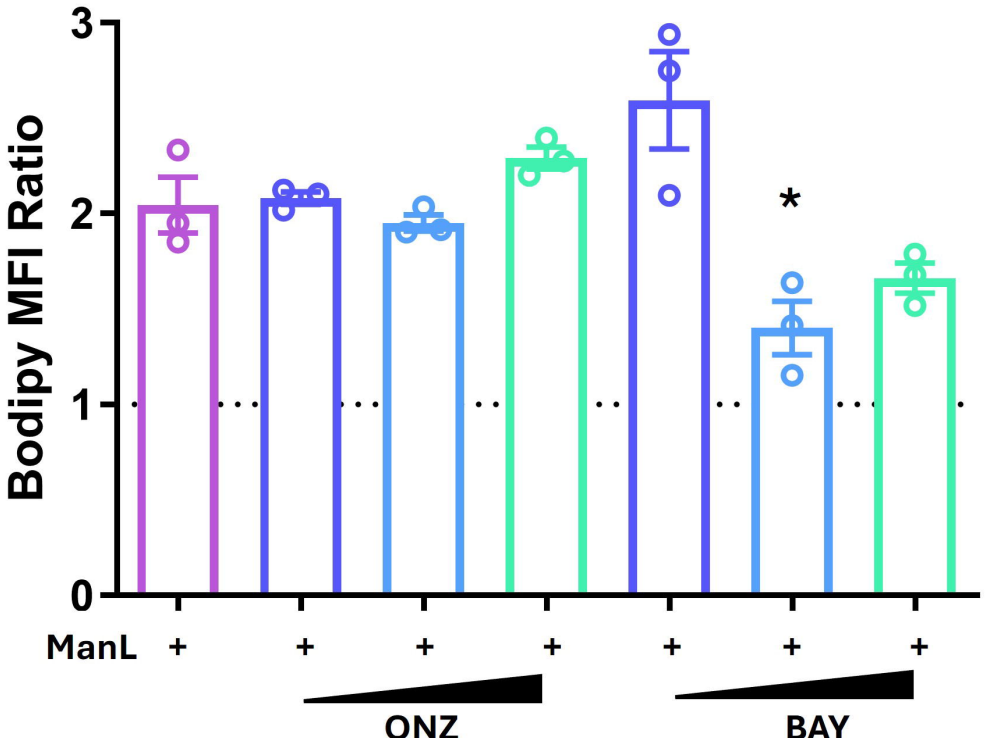
Figure S6